Excitons in Photosynthetic Purple Bacteria: Wavelike Motion or Incoherent Hopping?

Mirianas Chachisvilis, Oliver Kühn,† Tõnu Pullerits,* and Villy Sundström

Department of Chemical Physics, Chemical Centre, Lund University, P.O. Box 124, S-221 00 Lund, Sweden

Received: October 29, 1996; In Final Form: June 4, 1997[⊗]

We have studied excitation energy transfer in the photosynthetic antenna systems LH1 and LH2 of purple bacteria. Femtosecond pump−probe experiments are combined with computer simulations using the recently established crystal structure of these systems to assess the nature of excitation motion. We have measured the transient absorption kinetics and spectra of the LH1 and LH2 complexes in the temperature range from 4.2 to 296 K with femtosecond time resolution. The calculations based on the Pauli master equation disagreed with experimentally measured population and anisotropy kinetics, suggesting that the simple model of excitation hopping between bacteriochlorophyll *a* molecules is not a proper description for energy transport in LH1 and LH2. As a next step we have used the exciton theory to reproduce the transient absorption spectra of LH2, and we found that the coherence length of the exciton in B850 of LH2 1.5 ps after excitation of B800 is 4 ± 1.

1. Introduction

Primary processes in photosynthesis are the absorption of solar energy by antenna pigments and the transfer of excitation to photochemical reaction centers (RC), where the excitation is trapped in the form of a stable charge separation. Both the elementary excitation and electron transfer are ultrafast, leading to a quantum yield for the charge separation of almost 100%.

The antenna system of many photosynthetic purple bacteria consists of two different light-harvesting complexes, LH1 and LH2. The LH1 has a single absorption band with a maximum at about 880 nm (B880) and is directly connected with the RC. According to recent electron microscopic studies LH1 forms a ring of 16-fold symmetry, and the RC has been suggested to be located inside this ring.[1] The basic unit of this ring appears to be an α,β-polypeptide pair with two noncovalently bound bacteriochlorophyll (BChl) *a* molecules. The LH2 is a peripheral antenna with two distinct spectral bands—one with a maximum at 800 nm (B800) and another, depending on the bacterial species, somewhere from 820 nm to 850 nm (B850). Recently, the crystal structure of LH2 from *Rhodopseudomonas (Rps.) acidophila* was determined to a resolution of 2.5 Å, revealing a ring of nine α,β-polypeptide pairs, each containing two BChl *a* molecules of B850 and one BChl *a* of B800.[2]

Hopping-like Förster transfer and exciton state relaxation are two limiting cases of the general description of excitation dynamics. Which of them is actually observed in experiment depends on the coupling parameters and the dephasing in the studied system. Intermolecular excitation transfer in photosynthesis is generally described by the Förster dipole−dipole resonance mechanism. Measurements with relatively limited time resolution of the transfer between spectrally different antenna forms[3,4] and energy migration among similar pigment molecules have been described well by this incoherent hopping theory.[5−8] On the other hand, also the exciton concept has been applied to photosynthetic antenna systems.[9−11] In that case excitation is delocalized over a number of pigment molecules, and the dynamics occurs through the relaxation between different exciton states. However, often it is not so straightforward to unambiguously distinguish in experiment the two qualitatively different kinetic processes, and the actual dynamics can be a combination of these special cases. For example, smaller sections of the full system might behave as a small exciton whereas the dynamics on a larger scale may correspond to the hopping-like transfer of this small exciton. An argument against the pure incoherent Förster mechanism is the recent observation of coherent nuclear motions in the antenna complexes of photosynthetic bacteria.[12] The vibrational coherence is preserved for approximately the same time as the estimated single step transfer time in these systems. It means that one of the main assumptions of the Förster theory, that the vibronic relaxation occurs much faster than the excitation transfer, is apparently not fulfilled. Furthermore, the structural data[2] show a densely packed chlorophyll protein system, where exciton interactions are quite strong. Thus, the energy transfer in the purple bacteria is likely to initially involve a coherent stage, in which the excitation is delocalized over several molecules, while at longer time scales there will be incoherent hopping followed by trapping of the excitation in the RC.

In a recent work[13] we have found that at room temperature the elementary excitation in LH2 of the photosynthetic purple bacterium *Rhodobacter (Rb.) sphaeroides* 2 ps after excitation into the B800 band is an exciton of four BChl *a* molecules. In the current article we extend the above study. We present comprehensive transient absorption and anisotropy decay studies. With 40 fs time resolution we have measured transient absorption spectra and isotropic and anisotropic pump−probe decays in the B850 and B880 bands of the antenna complexes in the temperature range 4.2−295 K. Simulations using an incoherent hopping model are used to calculate the initial excitation dynamics. We also apply exciton theory to assess the coherence length of the exciton at different temperatures by simulating the transient absorption spectra.

2. Materials and Methods

Membranes of mutants of *Rb. sphaeroides* lacking either the core or peripheral light-harvesting complex were dissolved in buffer solution (Tricine 50 mM, pH 8) and diluted with 50−60% of glycerol to assure good optical quality of the sample glass at low temperature.

The excited state dynamics of the studied light-harvesting complex were measured using both one- and two-color pump−

† Present address: Institut für Physikalische und Theoretische Chemie, Freie Universität Berlin, Takustrasse 3, D-14195 Berlin.

[⊗] Abstract published in *Advance ACS Abstracts,* August 1, 1997.

S1089-5647(96)03360-3 CCC: $14.00

probe techniques. In the one-color experiments the excitation and probing pulses were generated using a regeneratively mode-locked Ti:sapphire laser, pumped by an argon ion laser. The output from this laser was ~1 W at a repetition rate of 82 MHz, and to prevent buildup of long-lived photoproducts, the pulse repetition rate was reduced to 40 kHz by using an acoustooptical pulse selector. The pulses were further attenuated to excitation intensities of $<1 \times 10^{14}$ photons/cm^2 per pulse. Compensation for wavelength chirp was performed in a two-prism compressor and resulted in transform limited pulses with a typical duration of 75 fs at 789 nm. The transient absorption anisotropy was calculated from the traces measured with parallel and perpendicular polarisations of the pump and probe pulses according to the formula $(I_{||} - I_{\perp})/(I_{||} + 2I_{\perp})$. Test measurements performed on the dyes IR140 and IR132 gave the expected result that anisotropy was 0.39 ± 0.03 on the time scale of a few picoseconds.

Transient absorption spectra were measured in a two-color pump−probe setup using for excitation ~70−100 fs pulses at 800 nm from an amplified (5 kHz) Ti:sapphire laser system. A white-light continuum generated in a 1 cm path length water cell was used for probing. The dual beam detection system based on a three-photodiode arrangement had a sensitivity (in ΔA) of $\sim 5 \text{ m} \times 10^{-5}$ by averaging the data from ~2000 pulses. The group velocity dispersion of the white-light pulse in the collimating and focusing optics led to a ~1 ps chirp in the 800−900 nm wavelength range. Therefore, the transient absorption spectra were recorded with simultaneous adjustment of the delay between probe and pump pulses to compensate for this chirp. The excitation intensity was $\sim 1 \times 10^{14}$ photons/cm^2, and the polarization of the pump light was set at the magic angle (54.7°) with respect to the probe. The optical density of the sample was usually chosen to be below 0.5/mm. The low-temperature measurements of the transient absorption spectra were performed using plastic cells with 3 mm optical path length, while for anisotropy measurements we used glass cells with 1 mm optical path length.

3. Results

A. LH1. *Kinetics and Anisotropy Decay.* In Figure 1 we present typical one-color transient absorption kinetics of the LH1 complex in its native membrane environment, excited and probed with 40−50 fs pulses centered at 888 nm at room temperature. It should be noted that the spectral width of such a short light pulse is around 370 cm^{-1}, which is close to the fwhm of the main absorption band of LH1 at room temperature (590 cm^{-1}) and even exceeds it at 4.2 K (290 cm^{-1}). Therefore, the spectral resolution of this type of measurements is low, but it is nevertheless sufficient for our purposes since we investigate processes that occur on the 50−100 fs time scale and consequently are accompanied by the lifetime broadening of the order of ~200 cm^{-1}. Figure 1 shows the transient absorption kinetics of the probe pulse measured using three different orientations of the pump pulse polarization with respect to the polarization of the probe: parallel, perpendicular, and magic angle (54.7°). The measurements performed with different excitation pulse energies and at different pulse repetition rates revealed no intensity dependence of the kinetic behavior, indicating that the excitation intensities were below the onset of singlet−singlet annihilation, and thus the measured kinetics reflects the true response of the system. In Figure 1 we also show the "raw" anisotropy obtained from the parallel and perpendicular components of the pump−probe signal. In order to quantify the experimental results, we have fitted the decays with a function, representing the convolution of the instrumental response

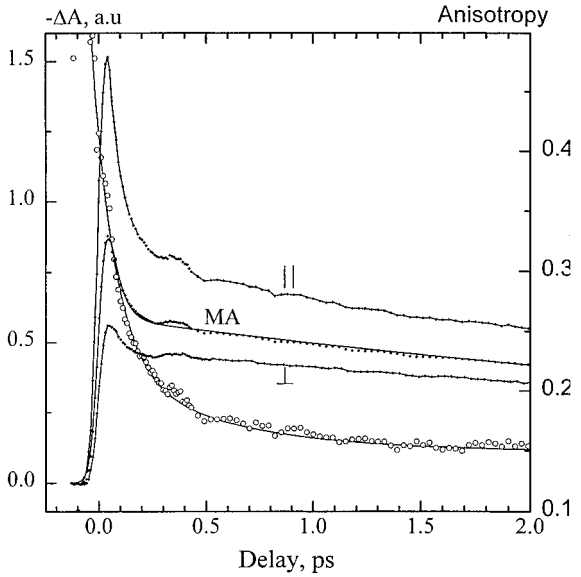

Figure 1. Transient absorption response and anisotropy of LH1 at room temperature after excitation with a 50 fs pulse centered at 888 nm. Parallel, perpendicular, and isotropic (magic angle) components of the pump−probe signal are shown separately. The solid lines are the fit to the isotropic signal and the anisotropy.

function with a sum of exponential decays. The parameters of the fit are summarized in Table 1. The fit to the isotropic signal (at the magic angle) revealed two distinct decay components: one very fast (~45 fs) and one much slower (~6 ps). It should be mentioned here that the accuracy of our data allows reliable deconvolution of components that are up to 2 times shorter than the fwhm of the instrumental response function. In order to fit the transient anisotropy ($r(t)$), we have made use of the relations $I_{\times fall} = {}^1/_3 I_{iso}(1 + 2r(t))$ and $I_{\perp} = {}^1/_3 I_{iso}(1 + r(t))$. The isotropic signal (constructed according to $I_{iso} = I_{||} + 2I_{\perp}$) was fitted first, and then a simultaneous fit to both the parallel and perpendicular components of the signal was performed, whereby $r(t)$ was modeled as a sum of exponential decays. The parameters of the fit to the anisotropy decay, shown in Figure 1, are detailed in Table 1. The main result is that the relaxation of the anisotropy is biphasic, with a fast (~100 fs) decay component and a slower (~560 fs) decay component.

According to the fit, the anisotropy decays from an initial value of ~0.46 to a final value of ~0.15. At room temperature these values vary slightly with pulse wavelength (data not shown), but the time constants remain approximately the same. This variation is mainly caused by the contribution from an excited state absorption that is strongly wavelength dependent. Generally, a small contribution from excited state absorption to a signal dominated by bleaching/stimulated emission (BL/SE) will lead to a higher value of the observed anisotropy (provided the transition dipole moments are not parallel). It is important to notice that the fast anisotropy decay component (~100 fs) is at least 2 times slower than the fast isotropic decay component (~45 fs) (vide infra).

In Figure 2 we show the transient anisotropy decays of the LH1 measured at $T = 4.2$ and 250 K in the red tail of the steady state absorption band, where the contribution from the excited state absorption (ESA) is negligible. The fits were performed as described above, and the parameters are detailed in Table 1. The results indicate that in the very red tail of the absorption band and at $T = 4.2$ K the anisotropy decay is significantly slowed down and can be well fitted with one exponential with a lifetime of ~1.9 ps and a final anisotropy value of approximately 0.25. At the same time the isotropic signal exhibits no decay at all on the relevant time scale of a few picoseconds.

TABLE 1: Summary of the Fit Parameters for the LH1 Complex

		isotropic decay fit				anisotropy fit				
T, K	λ, nm	τ_1, ps	A_1, %	τ_2, ps	A_2, %	τ_1, ps	r_1	τ_2, ps	r_2	r_∞
4.2	915	~200	100			1.9	0.04			0.32
50	915	~200	100			0.3	0.09	3.6	0.06	0.22
250	915	0.04	62	17	38	0.21	0.16	1.1	0.05	0.13
4.2	905	0.03	60	40	40	0.15	0.37	1.5	0.07	0.1
296	888	0.045	61	6	39	0.1	0.24	0.56	0.07	0.15

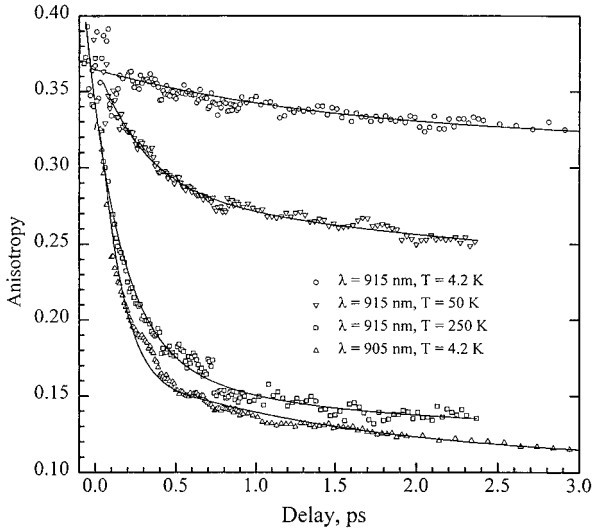

Figure 2. Transient absorption anisotropy of LH1 at different wavelengths and temperatures. The solid lines are the fit.

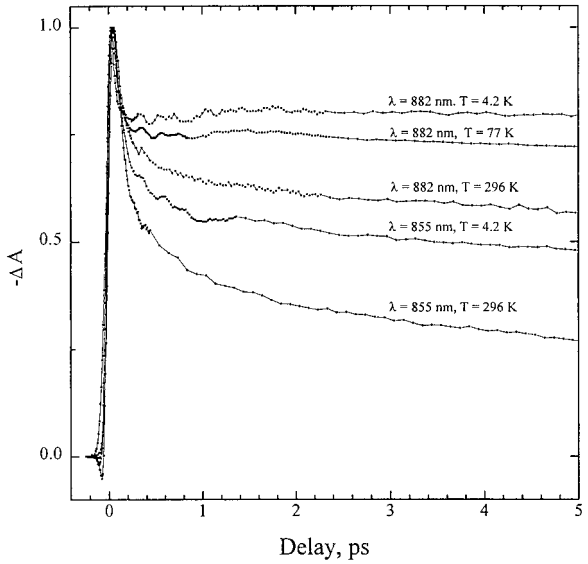

Figure 3. Time-resolved isotropic pump−probe signal of LH2 at different wavelengths and temperatures.

We further observe in Figure 2 that at higher temperatures the anisotropy relaxation occurs faster, and the decay becomes increasingly biphasic with the appearance of a very fast decay component with a characteristic lifetime on the order of 0.1−0.3 ps (see Table 1 for details). The lifetime and the amplitude (~0.05) of the slower picosecond anisotropy component do not change noticeably upon increase of the temperature, while the final anisotropy (r_∞) decreases to levels that are slightly higher than reported earlier by Bradforth *et al*. from fluorescence up-conversion studies.[14] The isotropic signal undergoes little change in the temperature range 4.2−50 K, but at higher temperatures it becomes much faster and notably nonexponential with a dominating lifetime of ~40 fs ($A = 60\%$) at $T = 250$ K.

Another important experimental observation that follows from the data in Figure 2 and Table 1 is that the shift of the pulse wavelength to the blue has a similar effect as a rise of the temperature. At 905 nm (and shorter wavelengths up to 888 nm) and at $T = 4.2$ K, both isotropic and anisotropy decays are almost as fast as at room temperature and also essentially biphasic, with a major ~30 fs decay component of the isotropic signal and a main ~150 fs decay component of anisotropy. However, at even shorter wavelengths the initial part of the pump−probe signal is dominated by a very short-lived (≤20 fs) induced absorption of the probe pulse, which masks the initial decay of anisotropy.[15]

B. LH2. *Kinetics and Anisotropy Decay.* Figure 3 shows isotropic one-color transient absorption kinetics of the LH2 complex in its native membrane environment measured with ~40−50 fs pulses at different temperatures and wavelengths. The data were fitted with a sum of two or three exponential decays. Optimized fitting parameters are summarized in Table 2. It is evident from the traces in Figure 3 that at low temperatures the initial dynamics shows some oscillatory motion involving a few modes with different frequencies. These oscillations are not further analyzed or discussed here, and for more details we refer to our recent work on this topic.[12,16] With the exponential deconvolution used here we do not intend to fit the oscillatory part of the decay, we use it here only to quantify the monotonically decaying part of the kinetics and to facilitate the comparison with the calculations. At these wavelengths the dominant contribution to the signal comes from the BL/SE (see below). A brief glance at the data reveals that relaxation after excitation into the long-wavelength side of the absorption band is clearly nonexponential, with dominating (~50 fs, $A \approx 60\%$) fastest decay component and a much slower component (40−800 ps, $A \approx 35\%$). In some traces also a very weak (0.6−5 ps, $A = 5\%$) component could be resolved. The measurements at different temperatures showed that the fastest (~50 fs) relaxation phase is weakly temperature dependent (in contrast to LH1), yet the overall relaxation is slowed down at low temperature because of the slower relaxation at later times. When the light pulses are tuned to shorter wavelengths (~855 nm), closer to the middle of the absorption band, the overall relaxation of the signal becomes faster even at $T = 4.2$ K; at the same time the fast initial decay phase seems to become slightly longer (100−130 fs) in this wavelength region. In Figure 4 we show the corresponding anisotropy decays of LH2 calculated directly from the parallel and perpendicular components of the pump−probe signal. Clearly, the relaxation is biphasic (within the accuracy of our measurements) and can be well fitted with a biexponential decay function. The fit parameters are summarized in Table 2. On the long-wavelength side (at ~882 nm) the initial depolarization proceeds with a 140−200 fs time constant that is almost temperature independent. However, the amplitude of this component increases from 0.13 to 0.2 when the temperature is changed from 77 K to room temperature. (The initial value of the anisotropy is ~0.33). In the low-temperature region from 4.2 to 77 K there are almost no observable changes in the depolarization process at all. It is worth mentioning that in this temperature range the steady state absorption spectrum (B850 band) is also weakly temper-

TABLE 2: Summary of the Fit Parameters for the LH2 Complex

		isotropic decay fit						anisotropy fit				
T, K	λ, nm	τ_1, ps	A_1, %	τ_2, ps	A_2, %	τ_3, ps	A_3, %	τ_1, ps	r_1	τ_2, ps	r_2	r_∞
4.2	882	0.05	60	5	2	180	38	0.14	0.11	6.8	0.07	0.15
77	882	0.04	55	800	45			0.2	0.13	6.4	0.05	0.16
296	882	0.05	61	0.6	5	46	34	0.2	0.2	6.0	0.04	0.09
296	864	0.07	52	13	48			0.1	0.28	2.2	0.04	0.09
4.2	855	0.13	56	2.5	8	91	36	0.07	0.16	1.3	0.03	0.09
296	855	0.1	56	1	11	26	32	0.06	0.4			0.2

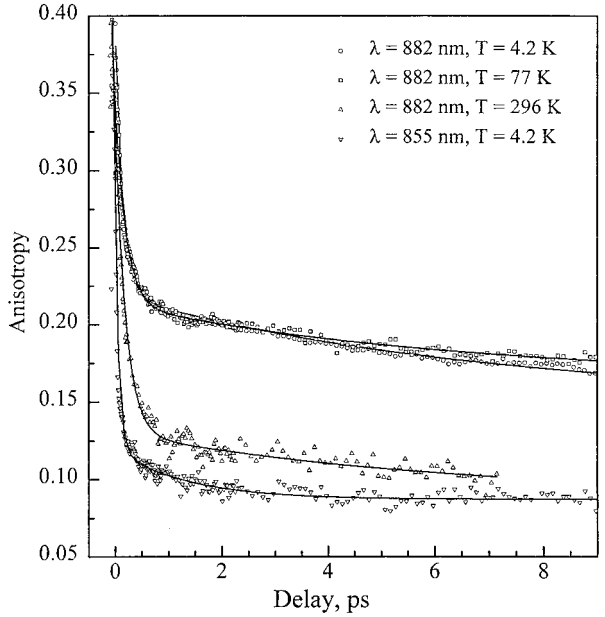

Figure 4. Transient anisotropy of LH2 at different wavelengths and temperatures. The solid lines represent biexponential fits to the data.

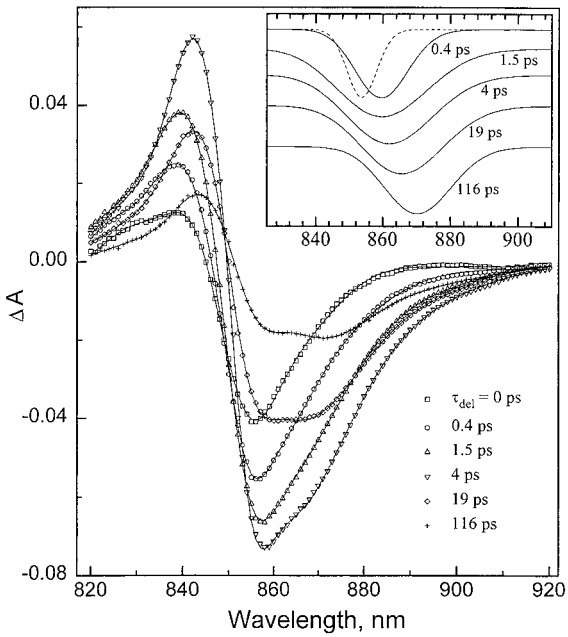

Figure 5. Transient absorption spectra of LH2 at different delay times after excitation at 800 nm and at 4.2 K. The solid lines represent multi-Gaussian fits. The inset displays the components of the fit representing the bleaching (no observable change with delay time, dash line) and stimulated emission contributions at different delay times.

ature dependent, whereas it red-shifts approximately 11 nm when going from 77 K to room temperature. At shorter wavelengths the initial anisotropy relaxation phase is accelerated further, to 60−70 fs irrespective of temperature. This is in contrast with isotropic decays that become slower at shorter wavelengths, in the vicinity of the absorption peak. The final values of the anisotropy are slightly higher than obtained by Jimenez et al.[17] from fluorescence up-conversion studies, which is likely to be due to the contribution from the ESA in our pump−probe measurements.

Transient Absorption Spectra of LH2. In Figure 5 we present the transient absorption spectra of the LH2 antenna recorded at different delay times after excitation with an ∼100 fs 800 nm pulse at $T = 4.2$ K. As a result of excitation into the B800 band, the initial spectral evolution is due to the B800 → B850 energy transfer, which leads to a rise of the BL/SE emission contribution in the vicinity of the B850 band. The time constant for this process at room temperature was earlier reported to be 0.7 ps[3,18] while 1.2 and 2.4 ps transfer times were obtained at 77[6,19] and 4.2 K,[20,21] respectively.

At larger delay times (≥4 ps) a new feature is observed in the transient spectra of Figure 5; the BL/SE emission band broadens and splits into two bands. It should be emphasized that this splitting is observed only at low temperature (4.2 K), and it is completely absent at room temperature. We have tried to fit the spectra with a sum of Gaussian functions in order to quantify the spectral changes. Generally one needs five Gaussian components to represent the transient spectra at large delay times; two of them are used to represent the ESA, and the other three account for the BL/SE contribution. In the inset of Figure 5 we plot the two most intense components of the fit to the BL/SE signal for different delay times. (The third component is less intense and is needed only to fit the long-wavelength tail of the spectra ≥890 nm.) A notable result of the fitting is that the component at 854 nm turned out to be approximately the same for spectra measured at different delay times (and is therefore plotted only for $\tau_d = 0.4$ ps), whereas the other component is shifting to longer wavelengths at larger delay times. We remind here that the steady state absorption spectrum of B850 peaks at ∼854 nm at 4.2 K. Therefore, it is tempting to interpret the component at 854 nm as a *bleaching* of the B850 band and the more long-wavelength component as a *Stokes-shifted stimulated emission*. The time scale of this shift can be estimated from the rising part of the kinetics measured at longer wavelengths where the BL contribution is minimal. Depending on the wavelength we obtained that the characteristic time constant for the Stokes shift lies in the range 3−8 ps. The appearance of this red-shifted band is much too fast to be bleaching and stimulated emission of the special pair of the reaction center, following energy transfer from the antenna. Here it is also interesting to note that the 4.2 K steady state fluorescence spectrum of a mutant of *Rb. sphaeroides* lacking both LH1 and RC is strongly red-shifted with a peak wavelength at ∼890 nm.[22] These authors assigned this emission to a minor long-wavelength component (BChl870) of B850.

In Figure 6A we present the transient absorption spectra of LH2 at different temperatures. The sample was excited at 800 nm with an ∼100 fs pulse and probed with continuum light pulses after 1.5 ps delay time. By this time the energy transfer step B800 → B850 is almost completed, but at the same time the shift of the SE is still small. We emphasize this point here

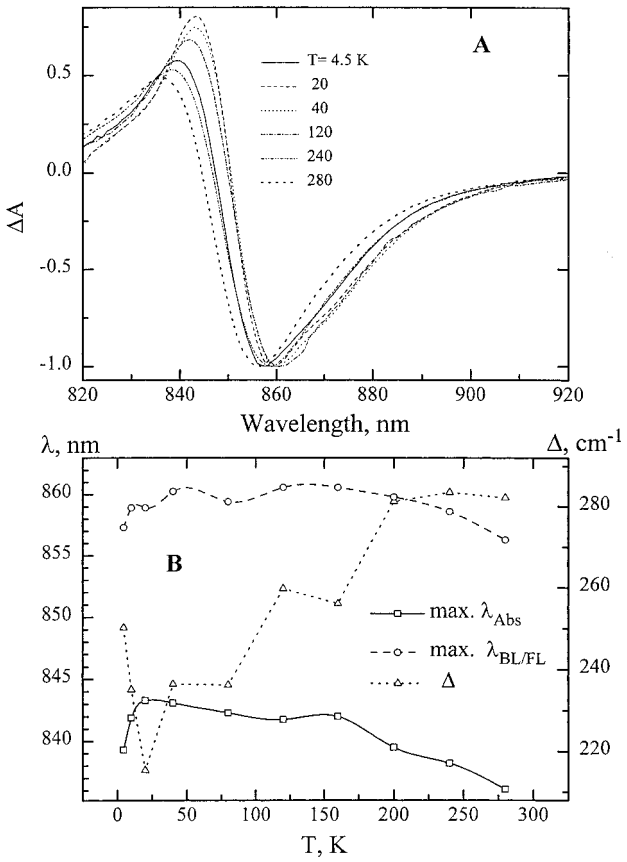

Figure 6. (A) Transient absorption spectra of LH2 at different temperatures and (B) the temperature dependence of the energy gap between the excited state absorption and the bleaching/stimulated emission. Open circles and dashed line are the variation with temperature of the bleaching/stimulated emission band maximum; open squares and full line are the corresponding variation of the maximum of the excited state absorption band, and open triangles and dotted line are the temperature variation of the energy gap (in cm^{-1}) between the two bands.

because of its importance for evaluation of the exciton size in the system (vide infra). The data show that upon cooling to ~50−20 K the BL/SE and ESA bands shift to the longer wavelengths, but at lower temperatures the direction of the shift is reversed (see Figure 6B). The spectral gap between the peaks of positive (ESA) and negative signal (BL/SE) decreases from 283 to 215 cm^{-1} upon cooling from room temperature to ~20 K and then rises to 250 cm^{-1} at 4.5 K. It is also worth noticing that the BL/SE band retains its width in a broad temperature range while the ESA band broadens at higher temperatures.

4. Numerical Simulations and Discussion

A. Incoherent Transfer Simulations. Our first approach is based on the assumption that energy migration between monomeric pigment molecules occurs via Förster-like hopping motion. The formalism for describing such dynamics can be found in a number of papers.[23,24] According to the Förster theory, the incoherent excitation transfer rate is proportional to the overlap integral of the emission spectrum of the donor and absorption spectrum of the acceptor.[25] In order to incorporate temperature dependence into the model, we have carried out simulations of the spectra of BChl *a* using the model described in ref 26. This model uses the linear harmonic Franck−Condon approximation and enables the calculation of the spectrum of the electronic transition that is coupled to vibronic modes and lattice phonons at any temperature. Here we are only interested in transfer inside of the inhomogeneous distribution function

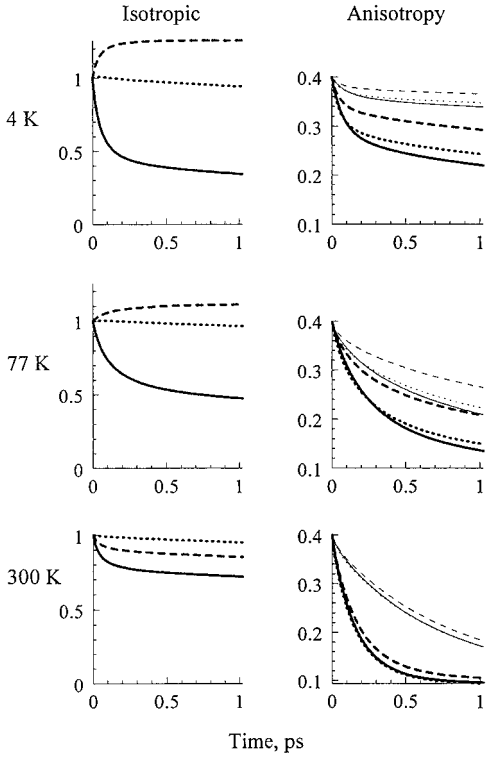

Figure 7. Simulated one-color pump−probe response of LH1 and LH2: isotropic and anisotropic decays at different temperatures and different wavelengths. Solid line, blue side of the spectrum (15 nm to the blue of the maximum); dotted line, center of the band; dashed line, red side of the band (15 nm to the red of the maximum). Thin lines represent anisotropy decays of LH1. The fwhm of the pulse spectrum is 300 cm^{-1}.

(IDF) of the site energies of a single spectral band. Therefore, the major part of the spectral overlap comes from the overlapping phonon wings, and we consider only the electron−phonon interaction, no vibrations are included. This is further justified by the fact that vibrational modes of chlorophyll-like molecules have very small Franck−Condon factors.[27] In the generalized master equation description of the excitation transfer the sharp zero phonon lines (ZPL) correspond to a slow decay of the memory functions.[28] In that way the overlap of ZPLs does not describe incoherent Förster transfer. In a simplistic way it can be visualized as a transfer to the ZPL of an acceptor where there is nowhere to relax at low temperature, and one of the main assumptions of the Förster theory is not satisfied. Thus, we have left the overlap of the donor emission with the ZPL of the acceptor out of the calculation of the transfer rate.

We have performed calculations for rings of 18 and 32 molecules corresponding to the B850 ring of LH2 and LH1, respectively. The transition dipole moments of the molecules are taken from the recently obtained structures,[1,2] and the energies of the 0−0 electronic transitions are distributed according to the Gaussian IDF of 170 cm^{-1} half-width. In the calculations we also take into account the spectral width of the excitation pulse of 300 cm^{-1}. The transfer time between the nearest neighbors in LH2 with equal site energies at 300 K was chosen to be 50 fs in order to reproduce the experimentally observed ~200 fs anisotropy decay time at the red side of the B850 band. The other transfer times for different temperatures, energy gaps, orientation factors, and distances were scaled to this transfer time. We have simulated the kinetics of the isotropic and anisotropic pump−probe signals at the blue edge, center, and red edge of the absorption band at three different temperatures (4, 77, and 300 K; see Figure 7). In order to quantify the calculated kinetics, we have performed a single-

TABLE 3: Fit Parameters for Calculated Isotropy Decays of LH2 (B850) and LH1

T, K	λ, nm	$\tau_{1,\,ps}$	A_1	$\tau_{2,\,ps}$	A_2	background
4.2	blue	0.05	0.44	0.37	0.2	0.33
	center	25				
	red	0.036	−0.16	0.14	−0.09	1.25
77	blue	0.07	0.25	0.4	0.28	0.47
	center	25	1			
	red	0.05	−0.07	0.63	−0.06	1.13
300	blue	0.05	0.18	0.58	0.12	0.7
	center	25	1			
	red	0.06	0.08	1.7	0.13	0.77

or double-exponential fit to the theoretical traces; the parameters of these fits are detailed in Tables 3−5. At first we take a closer look at the calculated isotropic decays. First of all, we point out that isotropic decays do not depend on the size of the ring because the only difference is in minor changes of orientation factors which is negligible for the N values used here. At the blue side of the spectrum (solid line in Figure 7), at all temperatures one can see a fast decay component due to the transfer from initially excited high-energy molecules to other molecules that have lower excited state energy. At 4 K this fast component has the largest amplitude. At the center of the band (dashed line) the transfer takes place among nearly isoenergetic molecules, and therefore the fast components have a small amplitude and the decays are quite similar at different temperatures. (In fact, the fit yields a lifetime of ∼25 ps, which is the assumed decay constant to the ground state for a single molecule.) At the red side of the band the kinetics at different temperatures have qualitatively different behavior; at 4 and 77 K only a rising component is present which corresponds to the accumulation of the excitation to the redmost pigments which give a strong bleaching signal. At 300 K, due to efficient uphill energy transfer, one can see an apparent fast decay component. Corresponding kinetics at the center of the band do not have such a fast component because at the center initially the full IDF is almost homogeneously excited while at the red side the excitations are created only at the most long-wavelength-absorbing pigments.

The anisotropy decays are sensitive to the structure. At all wavelengths we see significantly different kinetics for different ring sizes. Interestingly, the fastest initial stage at all temperatures is at the center of the band. The effect is most pronounced at 77 and 4 K. At these temperatures the homogeneous spectra are so narrow that at the edges of the band it is rather unlikely that a molecule has a neighbor with good spectral overlap, implying not only that uphill energy transfer is slowed down but also that excitation can be "trapped" at the blue side of the band because almost all neighbors have so much lower energy that the spectral overlap is relatively small. At the center of the band the escape probability is much higher because there it is much more probable that the initially excited molecule has a neighbor with a good spectral overlap. The localization at the blue edge of the band is not really perfect; the transfer away from blue molecules is simply slower than at the center of the band. At the red edge of the band at 4 K a considerable amount of initially created excitation is really trapped, which is indicated by the high value (>0.2) of the constant level of anisotropy.

The comparison of the calculated decay constants presented in Tables 3−5 shows that the anisotropy decays on the red side of the absorption band at high temperature are significantly slower than the corresponding isotropic decays (by a factor of ∼10 in the case of LH1 and ∼3 in the case of LH2). On the other hand, it follows from the experimental data presented in Tables 1 and 2 that anisotropy decays only by a factor of 2−4 (for LH1) and ∼2 (for LH2) slower than the corresponding isotropic signals. (One should compare 250 K data at 915 nm for LH1 (Table 1) and 296 K data at 864 nm for LH2 (Table 2) with theoretical values in Tables 3 and 4). The disagreement between experimental data and simulations is seen also at other temperatures and shorter wavelengths. This suggests that the above model of incoherent hopping between single BChl *a* molecules cannot fully describe the experimentally observed dynamics.

TABLE 4: Fit Parameters for Calculated Anisotropic Decays of LH1

T, K	λ, nm	τ_1, ps	r_1	τ_2, ps	r_2	r_∞
4.2	blue	0.06	0.035	0.4	0.045	0.32
	center	0.05	0.04	0.5	0.04	0.32
	red	0.05	0.02	0.5	0.03	0.35
77	blue	0.06	0.02	0.5	0.2	0.18
		0.48	0.21			0.19
	center	0.05	0.02	0.55	0.18	0.2
		0.48	0.2			0.2
	red	0.6	0.16			0.24
300	blue	0.63	0.28			0.12
	center	0.6	0.28			0.12
	red	0.7	0.28			0.12

TABLE 5: Fit Parameters for Calculated Anisotropic Decays of LH2 (B850)

T, K	λ, nm	τ_1, ps	r_1	τ_2, ps	r_2	r_∞
4.2	blue	0.07	0.1	0.62	0.1	0.2
	center	0.05	0.09	0.5	0.08	0.23
	red	0.05	0.05	0.5	0.06	0.29
77	blue	0.14	0.1	0.48	0.18	0.12
	center	0.1	0.1	0.68	0.19	0.11
	red	0.05	0.04	0.5	0.17	0.19
300	blue	0.11	0.13	0.23	0.17	0.1
		0.17	0.3			0.1
300	center	0.14	0.25	0.56	0.05	0.1
		0.17	0.3			0.1
	red	0.2	0.3			0.1

It should be pointed out here that an unambiguous interpretation of the isotropic one-color pump−probe signals in the region where pump and probe pulses are overlapping is not a straightforward task because of possible contribution from a number of qualitatively different four-wave mixing schemes which do not have anything to do with excitation transfer.[29] At the same time this will not change our conclusion—still the kinetics cannot reflect the hopping between BChl *a* monomers. Furthermore, the pairwise transfer time 50 fs what we have used in order to obtain agreement with experimental isotropic kinetics at the red side of the absorption band is significantly slower than our estimates of this quantity using Förster theory and the structure of LH2.

B. Simulations of Excitonic Transient Absorption Spectra of the LH2 Complex. *Parameters.* In this section we use an approach based on the calculation of delocalized excitonic states to simulate our experimental transient absorption spectra at different temperatures. The details of the formalism can be found elsewhere.[9,13] We only point out that since a monomeric BChl *a* molecule is known to have a relatively strong excited state absorption in the region of the Q_y transition,[6,30] we have described the antenna complexes as aggregates of three-level systems. It has been shown recently that this can influence quite significantly the calculated induced absorption spectra of aggregates.[31] We have used for the ratio of the dipole moments of the intramolecular excited and ground state absorptions of BChl *a* the value 0.5[30] and assume that these dipole moments are parallel.[32] The monomeric induced absorption is located about 100 cm^{-1} to the blue compared with the Q_y transition.[6,30] We make use of structural data for LH2[2] and include all

interactions into the Hamiltonian (not only the nearest neighbor). It is assumed that the monomeric transition energies are inhomogeneously broadened and uncorrelated. This is incorporated into the calculations using a Gaussian IDF. Furthermore, the IDFs of the lower transition (from the ground to the first excited state) and of the upper transition (from the first to the second excited state) of each BChl *a* molecule are taken to be correlated. The interaction between the pigments is not known to a high degree of accuracy. Quite different numbers for that quantity have been proposed in various works.[10,13,17,33] The dipole−dipole interaction can be calculated as described in ref 13, using the formula

$$V = 5.04\mu^2\kappa/R^3 \tag{1}$$

where V is in cm^{-1}, μ is the dipole moment in debye, R is the dipole separation in nanometers, and κ is the orientation factor. $\mu = 6.4$ D measured for BChl *a* in acetone solution[34] yields a nearest-neighbor interaction of $\sim$412 cm^{-1} within an α,β-polypeptide and $\sim$317 cm^{-1} for the interaction between bacteriochlorophylls in adjacent polypeptides. However, eq 1 has to be adjusted for the differences in refractive index of acetone and protein, but at the same time the refractive index of the latter is not well established. The effect of the polarizable medium is not only the reduction of the Coulombic interaction but also the enhancement of the dipole moment. These two effects work in opposite directions[13] and are not easy to take rigorously into account. Furthermore, the possible dressing of the excited state with lattice deformations (polaron formation) via electron phonon interaction would lead to a factor $\exp(-S)$ in eq 1, where S is the Huang−Rhys factor.[35] We conclude that the nearest-neighbor interaction in B850 is most likely somewhere between 200 and 450 cm^{-1}. Therefore, besides V values calculated directly from eq 1, we have also carried out calculations with 2 times smaller interaction. Below we refer to these two cases as calculations with strong and weak interaction.

The transient absorption spectra are calculated assuming that excited one-exciton manifold is in thermal equilibrium. The stick spectra are averaged over several thousand sets selected randomly from the Gaussian IDF and convoluted with a Lorentzian homogeneous line shape.

Localization. It is known that the energetic disorder of the pigment molecules leads to localization of the electronic eigenstates.[36,37] In order to quantify the degree of localization of a state σ with wave function φ_σ, a participation ratio R_σ can be used

$$R_\sigma = \sum_n |\varphi_{\sigma n}|^4 \tag{2}$$

The inverse participation ratio is frequently used as a measure of the extent of delocalization of the excitonic state, commonly referred to as the delocalization length,

$$N_{\mathrm{d}}^{\sigma} = 1/R_\sigma \tag{3}$$

In the limiting case of large inhomogeneity ($\Delta \gg V$), $N_{\mathrm{d}}^{\sigma} \rightarrow 1$. We note, however, that for a ringlike structure in the absence of disorder, $N_{\mathrm{d}}^{\sigma} < N$; i.e., it is smaller than the physical length of the complex. $N_{\mathrm{d}}^{\sigma} = N$ only for the lowest exciton state and if N is even then also for the highest state. All other doubly degenerate states give $N_{\mathrm{d}}^{\sigma} = {}^2/_3 N$. Therefore, N_{d}^{σ} can only serve as an approximate measure of the coherence length in the system. In fact, the eigenstates of the excitonic Hamiltonian are coherent superpositions of all the monomeric states of the whole ring no matter how large is the static disorder. The origin of the loss of phase relationship (coherence) in the system is the dynamic disorder induced by nuclear motions.

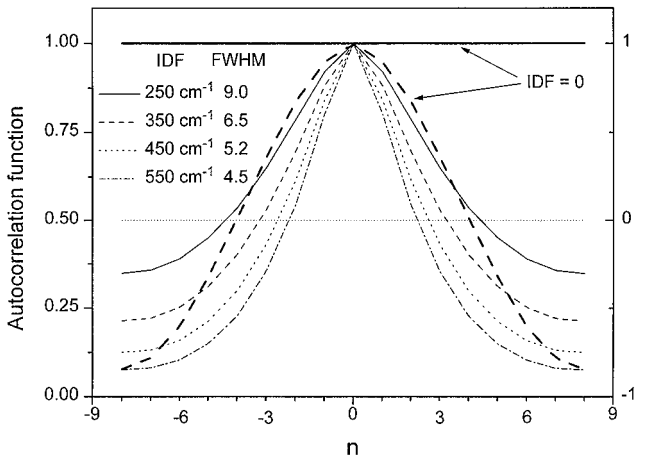

Figure 8. Calculated autocorrelation functions of the wave functions of the B850 ring. Thick lines (*y*-axis to the right) are without disorder. Solid line is for the lowest exciton level, and dashed line is for the second strongly allowed doubly degenerate level. Thin lines correspond to the lowest exciton state with different amounts of static diagonal disorder. The fwhm of the IDF are 250, 350, 450, and 550 cm^{-1}. The fwhm of the resulting autocorrelation functions are 9, 6.5, 5.2, and 4.5.

In following we have also characterized the extent of delocalization via the autocorrelation function of the wave function φ_σ of the state σ

$$F_\sigma(n) = \langle \sum_i \varphi_{\sigma i}\varphi_{\sigma i+n} \rangle \tag{4}$$

where $\langle\ \rangle$ denotes an average over the different configurations of the diagonal disorder and the index i runs over monomeric excitations. In the absence of disorder only the lowest exciton state has a constant autocorrelation function. Next to this state, two strongly allowed degenerate states give a cosine as the autocorrelation (see Figure 8). If one now takes the width of that function as a measure of the delocalization, then one could conclude that these states are delocalized over half the ring ($N_{\mathrm{d}} = 9$); the inverse participation ratio gives for the same states $N_{\mathrm{d}} = 12$. At the same time we know that the states are actually coherently delocalized over the full ring. We see that one has to be cautious assigning to such numerical quantities a significant physical meaning. All eigenstates of the Hamiltonian have the same extent of coherence, and therefore we have chosen the autocorrelation function of the lowest exciton state as a measure of the coherence length in the system since this state correctly indicates the full delocalization for $\Delta = 0$. The results of the calculations with strong interaction (see above) for four different Δ values (250, 350, 450, and 550 cm^{-1}) are presented in Figure 8. We can clearly observe that in case of large disorder the correlation of the states is decreasing rapidly. The delocalization lengths calculated as the fwhm of the autocorrelation function of the lowest exciton state give the following results: 9, 6.5, 5.2, and 4.5 for Δ values 250, 350, 450, and 550 cm^{-1}. Corresponding values for the inverse participation ratio (3) averaged over all the states are 10.2, 9.2, 8.2, and 7.4.

Comparison with Experiment. In order to investigate the temperature dependence of the delocalization length of the excitons in B850, we have compared the experimental absorption difference spectra measured at different temperatures with model calculations (see Figure 9). We found that the temperature dependence of the spectra can be well reproduced by only

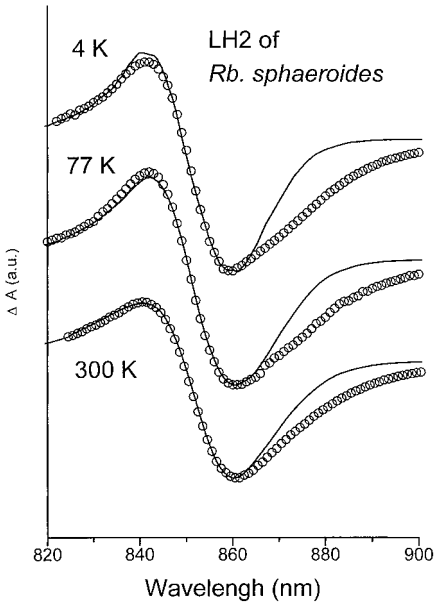

Figure 9. Experimental (circles) and calculated (lines) transient absorption spectra of LH2 at three different temperatures. Experimental spectra are recorded 1.5 ps after excitation at 800 nm. Calculations are carried out with weak interaction ($V = 200$ cm^{-1}), fwhm of the IDF is 550 cm^{-1}, and homogeneous widths are 25, 50 and 75 cm^{-1} for 4, 77, and 300 K, respectively.

varying the homogeneous spectral widths using the same width of the IDF of the site energies for all temperatures. In Figure 9 we present the experimental (circles) and calculated absorption difference spectra at three temperatures. The calculations are performed with weak interaction, the fwhm of the IDF is 550 cm^{-1}, and the homogeneous spectral widths that give the best fit are 25, 50, and 75 cm^{-1} for 4, 77, and 300 K, respectively. The calculations assuming strong interaction, with the fwhm of the IDF equal to 650 cm^{-1} (not shown), also lead to a good agreement with experiment. Here we point out that this width of the IDF should not be confused with the inhomogeneous broadening of the B850 absorption band since our inhomogeneous distribution is introduced as a diagonal disorder before Hamiltonian diagonalization. The inhomogeneous broadening of the absorption band is much smaller because of the motional narrowing. From the comparison between measured and calculated spectra in Figure 9 it can be seen that our calculations do not reproduce the red wing of the spectra. This is mainly due to the effects discussed in relation to Figure 5 and does not influence the fit to the ESA and bleaching part of the spectra.

Plots of the autocorrelation function of the lowest exciton state for the weak and strong interaction with the widths of IDF that gives the best fit to experimental absorption difference spectra are presented in Figure 10. The exciton delocalization length evaluated as the fwhm of this function is 2.9 and 4.0 for weak and strong interaction, respectively. The corresponding inverse participation ratio (3) averaged over all the states is 4.6 and 6.7. Since the autocorrelation function provides a clear visualization of the exciton delocalization concept, we have chosen this presentation for characterizing the delocalization length of the exciton. At the same time we point out that the wings of the autocorrelation function are rather broad; therefore, the fwhm slightly underestimates the extent of delocalization in the system, and we believe that the full profile of the autocorrelation function is in fact the best measure of delocalization.

Our model does not explicitly include interaction with the thermal bath which leads to a rapid dephasing and localization of the excitons. One would expect that the influence of phonons

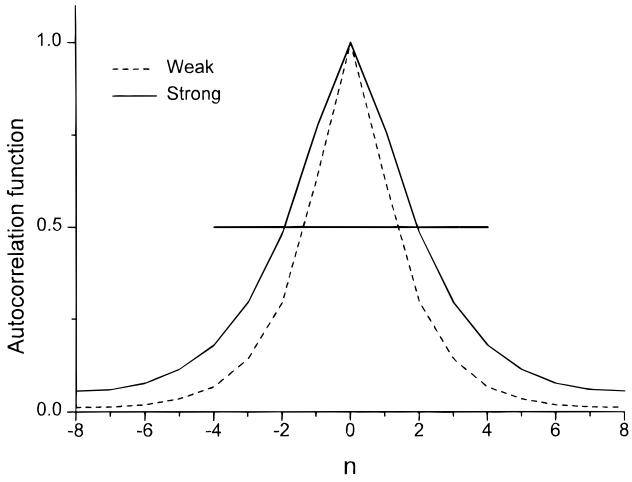

Figure 10. Autocorrelation function of the lowest state of B850 which corresponds to the best fit to the experimental spectra in case of strong ($V = 450$ cm^{-1}, solid) and weak ($V = 200$ cm^{-1}, dashed) interaction.

depends significantly on temperature, whereas the simulations and fits to the experimental results give the same delocalization length for all temperatures. (No change in IDF was needed at different temperatures.) On the other hand, in our experiment we deposit the excitation energy in the B800 pigment, and the excitation has gone through a relaxation process of more than 500 cm^{-1} when it ends up in B850. The local environment of the exciton 1.5 ps after B800 excitation might be quite hot even at 4 K which will accelerate the dephasing at the low temperatures. Also the zero-point nuclear motions may contribute to the dephasing. Furthermore, B800 to B850 transfer itself is almost certain to contribute to the localization of the B850 exciton, and the number of B850 molecules coupled to each monomeric B800 may limit the delocalization in our experiments. Direct optical excitation of B850 could, at least in a very early stage, give a different delocalization.

We formulate our conclusion here that the delocalization length of the exciton in B850 of *Rb. sphaeroides* 1.5 ps after excitation of B800 is 4 ± 1 BChl *a* molecules and does not significantly depend on the temperature. A very similar conclusion was reached by us recently[13] by using a much simpler model—we assumed that due to the dephasing the excitation is localized over a small part of the B850 ring, and the rest of the system was left out of the calculation. Those simulations were carried out without diagonal disorder, and the variation of the delocalization length was mimicked by changing the size of the system. The best fit to the experimental spectra was obtained by a segment of four BChl *a* molecules. The results of the current work appear to justify the approximations made in ref 13. We also note that in recent theoretical works by Leegwater[38] and Kühn et al.[39] it was concluded that the excitation, on the average, is delocalized over four BChl *a* molecules in LH1[38] and B850.[39] Excitonic effects at low temperature were also suggested by hole-burning studies.[21,40] Remarkably, in ref 40 even ringlike structure was proposed.

Concluding Remarks. In this work we have investigated the basic properties of the elementary excitations in the antenna system of purple bacteria. We have concluded that the appropriate description of this excitation is an exciton delocalized over four BChl *a* molecules. We have found that even at 4 K the delocalization length of the exciton is not significantly larger, suggesting that the zero-point nuclear motions may play a considerable role in dephasing processes at low temperature. Subsequent work with different excitation energies and careful study of transient absorption profiles at various early delay times

will hopefully give further insight into the time evolution and nature of the initial excited states in the photosynthetic light harvesting.

Acknowledgment. This work was supported by the Swedish Natural Science Research Council and EC Grant ERBCHBGCT 930361.

References and Notes

(1) Karrasch, S.; Bullough, P. A.; Ghosh R. *EMBO J*. **1995**, *14*, 631.
(2) McDermott, G.; Prince, S. M.; Freer, A. A.; Hawthornthwaite-Lawless, A. M.; Papiz, M. Z.; Cogdell, R. J.; Isaacs, N. W. *Nature* **1995**, *374*, 517.
(3) Shreve, A. P.; Trautman, J. K.; Frank, H. A.; Owens, T. G.; Albrecht, A. C. *Biochim. Biophys. Acta* **1991**, *1051*, 280.
(4) Hess, S.; Chachisvilis, M.; Timpmann, K.; Jones, M. R.; Fowler, G. J. S.; Hunter, C. N.; Sundström, V. *Proc. Natl. Acad. Sci. U.S.A.* **1995**, *92*, 12333.
(5) Pullerits, T.; Visscher, K. J.; Hess, S.; Sundström, V.; Freiberg, A.; Timpmann, K.; van Grondelle, R. *Biophys. J.* **1994**, *66*, 236.
(6) Hess, S.; Åkesson, E.; Cogdell, R. J.; Pullerits, T.; Sundström, V. *Biophys. J.* **1995**, *69*, 2211.
(7) Visser, H. M.; Somsen, O. J. G.; van Mourik, F.; Lin, S.; van Stokkum, I. H. M.; van Grondelle, R. *Biophys. J.* **1995**, *69*, 1083.
(8) Somsen, O. J. G.; van Mourik, F.; van Grondelle, R.; Valkunas, L. *Biophys. J.* **1994**, *66*, 1580.
(9) Pullerits, T.; Chachisvilis, M.; Jones, M. R.; Hunter, C. N.; Sundström, V. *Chem. Phys. Lett.* **1994,** *224*, 355.
(10) Novoderezhkin, V. I.; Razjivin, A. P. *FEBS Lett.* **1993**, *330*, 5.
(11) Somsen, O. J. G.; van Grondelle, R.; van Amerongen, H. *Biophys. J.* **1996**, *71*, 1934.
(12) Chachisvilis, M.; Pullerits, T.; Jones, M. R.; Hunter, C. N.; Sundström, V. *Chem. Phys. Lett.* **1994**, *224*, 345.
(13) Pullerits, T.; Chachisvilis, M.; Sundström, V. *J. Phys. Chem*. **1996**, *100*, 10787.
(14) Bradforth, S. E.; Jimenez, R.; van Maurik, F.; van Grondelle, R.; Fleming, G. R. *J. Phys. Chem.* **1995**, *99*, 16179.
(15) Chachisvilis, M.; Sundström, V. *J. Chem. Phys*. **1996**, *104*, 5734.
(16) Chachisvilis, M.; Fidder, H.; Pullerits, T.; Sundström, V. *J. Raman Spectrosc.* **1995**, *26*, 513.
(17) Jimenez, R.; Dikshit, S. N.; Bradforth, S. E.; Fleming, G. R. *J. Phys. Chem*. **1996**, *100*, 6825.
(18) Hess, S.; Feldchtein, F.; Babin, A.; Nurgaleev, I.; Pullerits, T.; Sergeev, A.; Sundström, V. *Chem. Phys. Lett.* **1993**, *216*, 247.
(19) Monshouwer, R.; de Zarate, I. O.; van Mourik, F.; van Grondelle, R. *Chem. Phys. Lett.* **1995**, *246*, 341.
(20) van der Laan, H.; Schmidt, Th.; Visschers, R. W., Visscher, K. J.; van Grondelle, R.; Völker, S. *Chem. Phys. Lett.* **1990**, *170*, 231.
(21) Reddy, N. R. S.; Small, G. J.; Seibert, M.; Picorel, R. *Chem. Phys. Lett.* **1991**, *181*, 391.
(22) van Dorssen, R. J.; Hunter, C. N.; van Grondelle, R.; Korenhof, A. H.; Amesz, J. *Biochim. Biophys. Acta* **1988**, *932*, 179.
(23) Pullerits, T.; Freiberg, A. *Biophys. J*. **1992**, *63*, 879.
(24) Jean, J. M.; Chan, C.-K.; Fleming, G. R.; Owens, T. G. *Biophys. J*. **1989**, *56*, 1203.
(25) Förster, Th. In *Modern Quantum Chemistry*; Sinanoglu, O., Ed., Academic Press: New York, 1965; Vol. 3, p 93.
(26) Pullerits, T.; Monshouwer, R.; van Mourik, F.; van Grondelle, R. *Chem. Phys.* **1995**, *194*, 395.
(27) Renge, I.; Mauring, K.; Avarmaa, R. *J. Lumin*. **1987**, *37*, 207.
(28) Kenkre, V. M.; Reineker, P. In *Exciton Dynamics in Molecular Crystals and Aggregates*; Springer-Verlag: New York, 1982.
(29) Chachisvilis, M.; Fidder, H.; Sundström, V. *Chem. Phys. Lett*. **1995**, *234*, 141.
(30) Becker, M.; Nagarajan, V.; Parson, W. W. *J. Am. Chem. Soc*. **1991**, *113*, 6840.
(31) Knoester, J.; Spano, F. C. *Phys. Rev. Lett*. **1995**, *74*, 2780.
(32) Savikhin, S.; Struve, W. S. *Biophys. J*. **1994**, *67*, 2002.
(33) Sauer, K.; Cogdell, R. J.; Prince, S. M.; Freer, A. A.; Isaacs, N. W.; Scheer, H. *Photochem. Photobiol*. **1996**, *64*, 564.
(34) Scherz, A.; Parson, W. W. *Biochim. Biophys. Acta* **1984**, *766*, 666.
(35) Dracheva, T. V.; Novoderezhkin, V. I.; Razjivin, A. P. *Chem. Phys*. **1995**, *194*, 223.
(36) Anderson, P. W. *Phys. Rev*. **1958**, *109*, 1492.
(37) Fidder, H.; Knoester, J.; Wiersma, D. A. *J. Chem. Phys*. **1991**, *95*, 7880.
(38) Leegwater, J. A. *J. Phys. Chem*. **1996**, *100*, 14403.
(39) Kühn, O.; Sundström, V. *J. Chem. Phys*., In press.
(40) Reddy, N. R. S.; Picorel, R.; Small, G. J. *J. Phys. Chem*. **1992**, *96*, 6458.